Gene expression cycles drive non-exponential bacterial growth

Arianna Cylke [1] and Shiladitya Banerjee [2,*]
[1]Department of Physics, Carnegie Mellon University, Pittsburgh, Pennsylvania 15213, USA
[2]School of Physics, Georgia Institute of Technology, Atlanta, Georgia 30332, USA

(Received 29 March 2025; accepted 25 June 2025; published 6 August 2025)

Bacterial populations typically exhibit exponential growth under resource-rich conditions, yet individual cells often deviate from this pattern. Recent work has shown that the elongation rates of *Escherichia coli* and *Caulobacter crescentus* increase throughout the cell cycle (super-exponential growth), while *Bacillus subtilis* displays a midcycle minimum (convex growth), and *Mycobacterium tuberculosis* grows linearly. Here, we develop a single-cell model linking gene expression, proteome allocation, and mass growth to explain these diverse growth trajectories. By calibrating model parameters with experimental data, we show that DNA-proportional mRNA transcription produces near-exponential growth, whereas deviations from this proportionality yield the observed non-exponential growth patterns. Analysis of gene expression perturbations reveals that ribosome expression primarily controls dry mass growth rate, whereas cell envelope protein expression more strongly affects cell elongation rate. We show that cell-cycle-dependent transcription dynamics give rise to convex, super-exponential, and linear modes of cell elongation observed experimentally, demonstrating how the timing of cell envelope and ribosomal protein expressions drive cell-cycle-specific behaviors. These findings provide a mechanistic basis for non-exponential single-cell growth and offer insights into how bacterial cells dynamically regulate elongation rates within each generation.

DOI: 10.1103/24rx-sxcw

I. INTRODUCTION

Early studies in bacterial growth physiology established that bacterial populations grow exponentially under nutrient-rich conditions where resources are not limiting [1]. Recent advancements in microfluidics and single-cell imaging technologies have enabled the collection of extensive, high-resolution single-cell datasets for bacterial growth [2–8]. These datasets have fueled the development of models addressing single-cell division control and size homeostasis [9–14], cell size control [13,15–17], shape maintenance [12,18–20], and adaptation to environmental changes [21–25]. Many of these models either assume exponential growth or overlook intragenerational dynamics. However, detailed analysis of high-resolution time-series data has revealed that elongation rates are not constant throughout the bacterial cell cycle. For instance, *Escherichia coli* [26,27] and *Caulobacter crescentus* [27,28] exhibit super-exponential growth, characterized by increasing elongation rates over the cell cycle. In contrast, *Bacillus subtilis* displays a convex elongation rate pattern, with a minimum rate near the midcell cycle [29], while *Mycobacterium tuberculosis* grows linearly [30]. To the best of our knowledge, no bacterial species has been reported to exhibit truly exponential elongation at the single-cell level. These observations raise the fundamental question of what drives these time-dependent growth patterns.

Cell growth is fundamentally driven by the translation of new proteins by ribosomes, with a variety of factors such as amino acid precursor and ribosome abundances influencing the rate at which overall protein translation occurs. Resource allocation models for the cellular proteome have been shown to be widely applicable for understanding bacterial growth from steady state [17,31–34] to dynamic environments [25,35–38]. According to the central dogma of molecular biology, genes are transcribed into mRNA, which is then translated by ribosomes to produce the protein mass of the cell [39]. For balanced exponential growth, the relative expression of genes determines the composition of the cell's proteome in a given environment [40], with constant gene expression and stable concentrations of mRNA and proteins [41]. Intuitively, non-exponential growth must involve deviations from these constant concentrations over the course of the cell cycle. Recent studies have revealed that transcription is linked to DNA replication, with transient increases in transcription occurring during the replication of specific genes [42,43]. Additionally, transcription rate is often assumed to be proportional to the DNA content of the cell [40,43]. Given that the duration of DNA replication does not always align with the cell cycle time [8], deviations from balanced exponential growth may not be surprising.

In this work, we examine how cell-cycle-dependent gene expression influences single-cell growth by combining proteome allocation theory and mRNA dynamics into a unified model. Building on existing models and guided by experimental data, we formulate a framework that explicitly includes two key sectors—ribosomes and the cell

*Contact author: sbanerjee347@gatech.edu

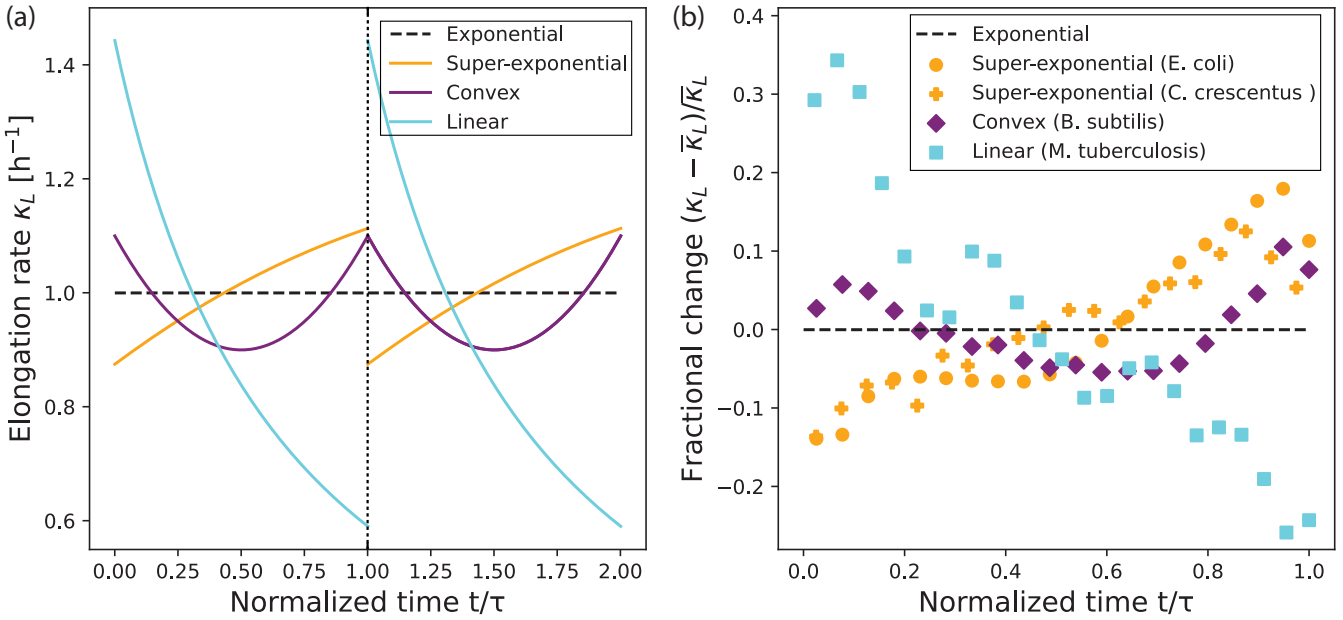

FIG. 1. Non-exponential elongation modes in bacterial cells. (a) Qualitative growth trajectories illustrating how various modes of bacterial growth deviate from purely exponential growth. The elongation rate $\kappa_L = L^{-1}dL/dt$ is plotted against normalized time t/τ for two cell cycles, where τ is cell cycle duration. (b) Ensemble-averaged elongation rate data for four representative bacterial cells of the growth modes illustrated in (a), plotted in normalized time. Individual cell elongation rate trajectories were extracted from length data via a trapezoidal derivative approximation and then averaged in bins of normalized time. For ease of comparison, we plot the fractional change in growth rate (where $\bar{\kappa}_L$ denotes cell cycle average). *E. coli* K12 NCM3722 cells are grown in supplemented Glucose media at 37 °C [4], *C. crescentus* cells are grown in PYE at 34 °C [12], *B. subtilis* BSB1 cells are grown in glycerol at 37 °C [8], and *M. tuberculosis* CDC1551 cells are grown in supplemented 7H9 growth medium at 37 °C [30].

envelope—treating nutrient availability and mRNA transcription rates as the primary input parameters. Initially, we find that transcription scaled to DNA content yields near-exponential growth, even with DNA concentration fluctuations throughout the cell cycle. However, this prediction does not match the non-exponential growth patterns observed in many bacterial species. Consequently, we introduce additional time-dependent transcription dynamics to better capture experimental findings. By systematically varying transcription rates, we quantify how these perturbations shape cell growth, both in general and within the context of cell cycle data. We further pinpoint the timescale limitations that govern how gene expression and downstream processes affect overall growth. Using these insights, we explain the mechanistic origins of non-monotonic elongation rate in *B. subtilis*, super-exponential growth in *E. coli*, and linear growth in *M. tuberculosis*, underscoring how trade-offs between ribosome and envelope synthesis vary over the cell cycle. Together, these findings provide a mechanistic understanding of the regulatory principles shaping bacterial growth dynamics at the single-cell level.

II. NON-EXPONENTIAL ELONGATION MODES OF SINGLE BACTERIAL CELLS

While bacterial population growth is often quantified by mass or optical density, single-cell growth data are collected via microscopy and image analysis. Consequently, single-cell growth metrics typically focus on morphological parameters, such as cell length and width. For the rod-like bacterial cells examined in this study, cell width remains approximately constant throughout the cell cycle; changes in cell length directly reflect growth. Hence, we characterize single-cell growth by the elongation rate, $\kappa_L = L^{-1}dL/dt$, which is constant for purely exponential growth. In practice, however, experimental time-lapse data do not show purely exponential growth in cell length trajectories.

Figure 1(a) shows qualitative examples of super-exponential (*E. coli*), convex (*B. subtilis*), and linear (*M. tuberculosis*) elongation rates, while Fig. 1(b) displays representative datasets from these species [4,8,12,30]. To facilitate cross-species comparisons—given their distinct growth timescales—we plot the fractional deviation from the mean elongation rate, $\kappa_L/\bar{\kappa}_L - 1$. Here, super-exponential growth appears concave and asymptotically approaches exponential behavior [27], whereas linear growth is convex. Notably, in *B. subtilis*, the convex growth pattern begins and ends each generation at approximately the same elongation rate, whereas super-exponential and linear growth modes are strictly monotonic, resetting to the initial rate after division. It is important to recognize that non-exponential growth at the single-cell level does not necessarily imply non-exponential population growth; as long as the cell cycle duration remains consistent across cells, the overall population still grows exponentially.

Despite these observations, our mechanistic understanding of non-exponential growth remains limited. Existing models of super-exponential and linear growth largely focus

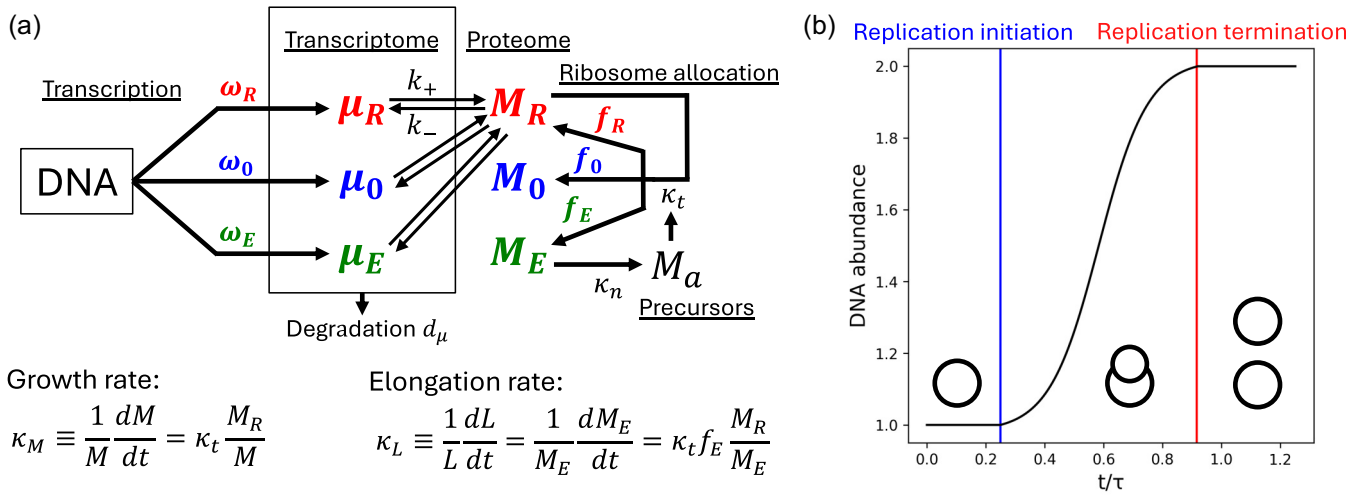

FIG. 2. Overview of the single-cell growth model. (a) Schematic illustrating how DNA abundance determines mRNA transcription rates, which then set mRNA levels for each proteome sector. The mRNA binds to ribosomes to determine the allocation fractions for each sector ribosomal, envelope, or "other") and degrades over time when unbound. Ribosomes grow the dry mass of the cell through translation of proteins in proportions set by the allocation fractions. The cell envelope mass sets the surface area and therefore the rate at which nutrients are imported, the abundance of which sets the transcription rate. (b) A representative DNA-replication logistic function describing DNA abundance in relative time, as defined in Eq. (12). Blue and red vertical lines mark replication initiation and termination, respectively, and the black circles depict the bacterial chromosome at different replication stages.

on cell-envelope processes, suggesting that *E. coli* elongates exponentially in only a subsection of the cell envelope [27], whereas *M. tuberculosis* grows exclusively at its poles [30]. For *B. subtilis*, the location of the midcycle minimum in elongation rate has been linked to cell size control [8]. However, these morphological models do not fully explain the underlying physiological mechanisms driving non-exponential growth. In particular, what do these patterns imply about gene expression and proteome changes within a single cell cycle? In subsequent sections, we place these distinct growth modes in the context of the central dogma of molecular biology, aiming to understand how non-exponential single-cell growth arises from temporal patterns of gene expression and proteome allocation.

III. MECHANISTIC MODEL FOR SINGLE-CELL GROWTH CONTROL

To explain the mechanistic basis for exponential and non-exponential bacterial growth at the single-cell level, we develop a theoretical framework that links gene expression to proteome allocation and nutrient uptake, ultimately driving single-cell growth (Fig. 2). We begin by adapting the well-established proteome allocation theory, which partitions the cellular proteome into ribosomal, envelope, and other protein sectors. We then couple this allocation to a dynamical description of mRNA transcription, ribosome binding, and protein synthesis. Next, we incorporate the role of DNA replication in modulating transcription rates and thus gene dosage. Finally, we outline how these biochemical processes translate into changes in cell morphology and growth, enabling direct comparison with experimental data. Together, these components provide a comprehensive mechanistic model of how time-dependent gene expression shapes bacterial growth at the single-cell level.

A. Proteome allocation

We begin by adopting a well-established proteome allocation framework for bacterial growth [31,32]. In such models, cell dry mass M increases through the translation of new proteins by ribosomes. If the translation rate is κ_t, then

$$\frac{\mathrm{d}M}{\mathrm{d}t} = \kappa_t M_R \tag{1}$$

where M_R is the abundance of ribosomes. Cell growth rate is defined as the relative growth rate of total cell mass,

$$\kappa_M \equiv \frac{1}{M}\frac{\mathrm{d}M}{\mathrm{d}t} = \kappa_t \frac{M_R}{M}. \tag{2}$$

In our model, we divide the proteome into three main sectors: (i) ribosomal proteins of mass M_R, the cell envelope (and periplasm) of mass M_E, and all other proteins of mass $M_0 \equiv M - M_R - M_E$. We define an allocation fraction f_q as the fraction of actively translating ribosomes devoted to synthesizing sector q. Accordingly,

$$\frac{\mathrm{d}M_q}{\mathrm{d}t} = \kappa_t f_q M_R. \tag{3}$$

Ribosomes not actively translating any sector are accounted for by a free ribosome mass fraction f_F. Thus, $f_R + f_E + f_0 + f_F = 1$ spans the entire proteome's translational allocation.

To track the changing distribution of mass between sectors, we introduce the mass fraction $\phi_q = M_q/M$. Combining the definition of ϕ_q with Eq. (3), we arrive at

$$\frac{\mathrm{d}\phi_q}{\mathrm{d}t} = \kappa_t (f_q - \phi_q)\phi_R. \tag{4}$$

Under steady-state conditions, constant allocations imply $f_q = \phi_q$. However, for time-varying $f_q(t)$, the instantaneous ϕ_q lags behind f_q, relaxing toward it at a rate set by $\kappa_t \phi_R$. As long as these allocation changes are cyclic and repeat each generation, the intergenerational average mass fractions $\bar{\phi}_q$ remain consistent—even if fluctuations arise within the cell cycle.

Bacterial cells can be limited by nutrient uptake, translation capacity, or a combination of the two. Cells grow optimally when they balance both of these limitations to maximize overall growth rather than translation speed or precursor abundance [32]. Our model incorporates these limitations by introducing an amino acid precursor pool of mass M_a. Flux balance implies

$$\frac{\mathrm{d}M_a}{\mathrm{d}t} = \kappa_n M_E - \kappa_t M_R, \tag{5}$$

where κ_n denotes the nutrient uptake rate. We assume that nutrient uptake is proportional to the cell envelope mass, consistent with uniform nutrient transport across the cell surface [44,45].

The translation rate κ_t decreases when the amino acid mass fraction $\phi_a = M_a/M$ is low, reflecting precursor scarcity. We capture this using

$$\kappa_t(\phi_a) = \kappa_{t,0} \frac{\phi_a^2}{\phi_a^2 + \phi_{a,t}^2}, \tag{6}$$

where $\kappa_{t,0}$ is the maximum translation rate, and $\phi_{a,t}$ sets the threshold at which precursor limitation attenuates translation. Similarly, nutrient uptake undergoes feedback inhibition at high ϕ_a,

$$\kappa_n(\phi_a) = \kappa_{n,0} \frac{\phi_{a,n}^2}{\phi_a^2 + \phi_{a,n}^2}, \tag{7}$$

with $\phi_{a,n}$ determining the threshold for uptake feedback and $\kappa_{n,0}$ the maximal uptake rate. The sigmoidal forms for $\kappa_t(a)$ and $\kappa_n(a)$ reflect that translation is significantly attenuated when the amino acid mass fraction falls below $\phi_{a,t}$, and the amino acid supply flux is strongly diminished by feedback inhibition for ϕ_a above $\phi_{a,n}$ [32]. Parameter values estimated for *E. coli* include $\phi_{a,t} = 10^{-4}$, $\phi_{a,n} = 10^{-3}$, and $\kappa_t^0 = 5.9\,\mathrm{h}^{-1}$ [32].

Although we primarily focus on cells in nutrient-rich conditions, explicitly including precursors in the model highlights the trade-off between ribosomes and the envelope. Allocating more resources to ribosomes increases the cell's overall translation capacity, while reducing envelope allocation limits nutrient uptake. Thus, our framework captures both translation-driven and nutrient-driven constraints in single-cell growth.

B. Gene expression dynamics

Allocation of proteome resources within the cell is governed by gene expression. In a minimal model, DNA is transcribed into mRNA, which then provides instructions for ribosomes to synthesize proteins. To connect gene expression to dynamic proteome allocation, we adapt the framework from Ref. [34], defining μ_q as the mRNA abundance for each proteome sector $q \in \{R, E, 0\}$. The corresponding time-evolution equation is

$$\frac{\mathrm{d}\mu_q}{\mathrm{d}t} = \omega_q(t) + \left(k_- + \frac{v_t}{n_q}\right) f_q \frac{M_R}{m_R} - \left(k_+ f_F \frac{M_R}{m_R M} + d_\mu\right)\mu_q, \tag{8}$$

where $\omega_q(t)$ is the time-dependent mRNA transcription rate, k_+ (k_-) is the rate of mRNA-ribosome binding (unbinding), v_t is the rate at which a single ribosome translates amino acids, n_q is the average number of amino acids per protein in the sector, m_R is the mass of a single ribosome, and d_μ is the mRNA degradation rate. Note that the term v_t/n_q corresponds to ribosome unbinding upon completion of protein synthesis. The equation governing the time-evolution of mRNA-ribosome complex is given by

$$\frac{\mathrm{d}}{\mathrm{d}t}\left(f_q \frac{M_R}{m_R}\right) = \left(\frac{k_+ \mu_q f_F}{M} - \left(k_- + \frac{v_t}{n_q}\right) f_q\right)\frac{M_R}{m_R} - f_q \frac{\dot{M}_R}{m_R}. \tag{9}$$

Using Eq. (3) to substitute for $\dot{M}_R$, we derive the time dependence of f_q,

$$\frac{\mathrm{d}f_q}{\mathrm{d}t} = \frac{k_+ \mu_q f_F}{M} - \left(k_- + \frac{v_t}{n_q} + 2 f_R \kappa_t\right) f_q. \tag{10}$$

Since $\sum_q f_q = 1$, we also have

$$\frac{\mathrm{d}f_F}{\mathrm{d}t} = -\sum \frac{\mathrm{d}f_q}{\mathrm{d}t}. \tag{11}$$

Most of these parameters are known for *E. coli*: $d_\mu = 6\,\mathrm{h}^{-1}$ [46], $k_- = 60\,\mathrm{h}^{-1}$, and $k_+ = 1.1 \times 10^5\,\mathrm{MDa/h}$ [34]. Ribosomes contain $n_R \approx 7459$ amino acids [47], so $v_t = n_R \kappa_t$, and each ribosome has a mass $m_R \approx 2.7\,\mathrm{MDa}$ [48]. Typical envelope or general proteome proteins have ~287–294 amino acids in *E. coli* and *B. subtilis* [49]. While n_R describes a complete ribosome, ribosome-affiliated proteins are translated individually, and thus we approximate $n_E = n_0 = n_R$ in Eq. (10). Consequently, the only remaining free parameters are the transcription rates $\omega_q(t)$, the maximal nutrient uptake $\kappa_{n,0}$, and the initial conditions used to integrate the system.

Figure 2(a) summarizes this framework in a schematic: DNA abundance sets the mRNA transcription rates $\omega_q(t)$, forming ribosome-mRNA complexes for each proteome sector (ribosomal, envelope, and "other"). The cell envelope then modulates nutrient uptake, which in turn affects the cell's amino acid pool and, consequently, translation. Note that our model does not optimize for growth rate by setting the values for transcription rates and ribosome allocation fraction. Instead, we allow suboptimal growth scenarios where translation rate is reduced owing to precursor scarcity or feedback inhibition. Figure 2(b) shows a sample logistic function for DNA abundance, with blue and red vertical lines marking initiation and termination of DNA replication that shape these transcription dynamics. Overall, this model links gene expression (via mRNA transcription) to proteome allocation, enabling us to study how changing transcription rates throughout the cell cycle impact bacterial growth dynamics.

C. DNA replication dynamics

Experiments indicate that transcription is roughly proportional to gene dosage, i.e., to the cell's DNA content [40,43].

Bacterial cells maintain a tightly controlled cell volume per replication origin, ensuring that DNA replication initiates at a specific cell size regardless of nutrient availability. For *E. coli*, this critical volume per origin is approximately $0.28\,\mu m^3$, while for *B. subtilis* it is approximately $0.60\,\mu m^3$ [8]. Certain bacterial species like *C. crescentus* tightly coordinate DNA replication with cell cycle and do not undergo multifork replication [50]. Implementing a cell-cycle-based initiation criterion for DNA replication would leave every other aspect of our framework intact, so the implementation outlined in Sec. IV still applies. The sole consequence is a possible shift in the predicted minima and maxima of growth and elongation rates compared with the model of DNA replication initiation at a critical cell volume.

Once replication begins, the C period (time interval between the initiation and termination of chromosome replication) τ_C can be considered to be growth rate independent under nutrient-rich conditions (i.e., for $\kappa \gtrapprox 0.7\,h^{-1}$). In *E. coli*, τ_C has been measured at 39 min [8], whereas *B. subtilis* exhibits a similar baseline of 40 min (although it shows a weak linear dependence on growth rate, fitted by $1.02\,h^{-1} - 0.26\,\kappa$ [8]).

Using these two parameters—the initiation time and the replication duration—we model the abundance of a single chromosome by a logistic function,

$$\mathrm{DNA}(t) = 1 + \frac{1}{1 + \exp\left[\alpha\left(t - \left(t_r + \frac{\tau_C}{2}\right)\right)\right]}, \tag{12}$$

where t_r is the time at which the initiation criterion (critical cell volume) is met, and $\alpha = \frac{8}{\tau_C}$ ensures that ∼98% of replication completes within the interval $t \in [t_r,\, t_r + \tau_C]$. As we will see further in Sec. IV, the initiation criterion and halving DNA content during cell division is sufficient to capture multifork replication. Consequently, the instantaneous transcription rate for mRNA in sector q can be written as

$$\omega_q(t) \;=\; \omega_q^* \cdot \mathrm{DNA}(t), \tag{13}$$

where ω_q^* is the transcription rate per chromosome. We term this *DNA-proportional transcription* model. Figure 2(b) shows a sample logistic curve illustrating this replication-driven modulation of $\omega_q(t)$ during one cell cycle.

D. Cell morphology and growth

To compare our model predictions with microscopy-based measurements, we approximate each bacterial cell as a cylindrical rod of length L and width w, with hemispherical end caps. The cell volume is given by

$$V \;=\; \frac{4}{3}\pi\left(\frac{w}{2}\right)^3 + \pi\,(L - w)\left(\frac{w}{2}\right)^2. \tag{14}$$

We can convert between cell morphology and mass using experimental measurements for the average dry mass density ρ. For instance, *E. coli* has $\rho \approx 0.30\,g\,ml^{-1} \approx 1.7 \times 10^5\,\mathrm{MDa}\,\mu m^{-3}$ [20], while *B. subtilis* has $\rho \approx 0.32\,g\,ml^{-1} \approx 1.9 \times 10^5\,\mathrm{MDa}\,\mu m^{-3}$ [51].

In rod-like bacteria, the cell envelope mass M_E is proportional to the total surface area of the cylinder and hemispherical end caps, $S = \pi\, w\, L$, which we write as $M_E \;=\; d\,\rho_E\,\pi\,wL$, where ρ_E is the envelope density and d its thickness. Consequently, the increase in M_E reflects the increase in L, so the cell's elongation rate can be expressed as

$$\kappa_L \;\equiv\; \frac{1}{L}\frac{\mathrm{d}L}{\mathrm{d}t} \;=\; \frac{1}{M_E}\frac{\mathrm{d}M_E}{\mathrm{d}t} \;=\; \kappa_t\, f_E\, \frac{M_R}{M_E}. \tag{15}$$

This definition allows direct comparison to experimental measurements of cell length. By contrast, the growth rate of total cell mass is

$$\kappa_M \;\equiv\; \frac{1}{M}\frac{\mathrm{d}M}{\mathrm{d}t} \;=\; \kappa_t \frac{M_R}{M}. \tag{16}$$

Hence, κ_L quantifies cell size elongation while κ_M quantifies how total cellular biomass increases over time.

IV. MODEL IMPLEMENTATION: EMERGENCE OF EXPONENTIAL GROWTH

We now describe how our single-cell growth model is numerically implemented, including the implementation of the cell division rule and intergenerational dynamics of cellular proteome and transcriptome. Using this model, we show that transcription rates scaling with cellular DNA content naturally lead to near-exponential growth, even when DNA replication is not strictly synchronized with cell mass.

To simulate how single cells evolve their size, growth rate, and proteome composition across generations, we explicitly incorporate cell division in our simulations. At the beginning of the first simulated cell cycle, we specify the initial values for each sector's mRNA abundance μ_q, total mass M_q, allocation fractions f_q, and mass fractions ϕ_q. These quantities then converge to their homeostatic values over multiple generations, consistent with homeostasis in cell size and growth rate. In particular, we implement an "adder" rule for cell size regulation and division control, supported by experimental data showing that rod-shaped bacteria add a constant length (and therefore a constant envelope mass M_E) between divisions, regardless of birth length [4,8,10]. Once the cell meets its division criterion, we implement symmetric division by halving each extrinsic quantity (μ_q, M_q, and L) in daughter cells. The final values of f_q and ϕ_q at division become the initial values for the daughter cells in the next generation.

Next, we detail how the model equations are integrated and how DNA replication is coupled to transcription. At each timestep during the cell cycle, we dynamically update:

(1) The DNA content, using Eq. (12), whenever the cell meets the initiation mass threshold. For cells undergoing multifork replication, the process is identical with summed contributions from each chromosome.
(2) The sector-specific mRNA abundances $\mu_q(t)$ via Eq. (8), where $\omega_q(t) = \omega_q^* \cdot \mathrm{DNA}(t)$ sets the instantaneous transcription rate.
(3) The proteome allocation fractions $f_q(t)$ using Eqs. (10) and (11).
(4) The sector masses $M_q(t)$ using Eqs. (1) and (5).
(5) The mass fractions $\phi_q(t) = M_q(t)/M(t)$ using Eq. (4).

If multifork replication has not completed by the time of cell division, we allow the unfinished replication forks to continue in the next generation, assuming equal partitioning of chromosomes upon division. Regardless of the initial DNA content, the number of origins and replication forks at steady

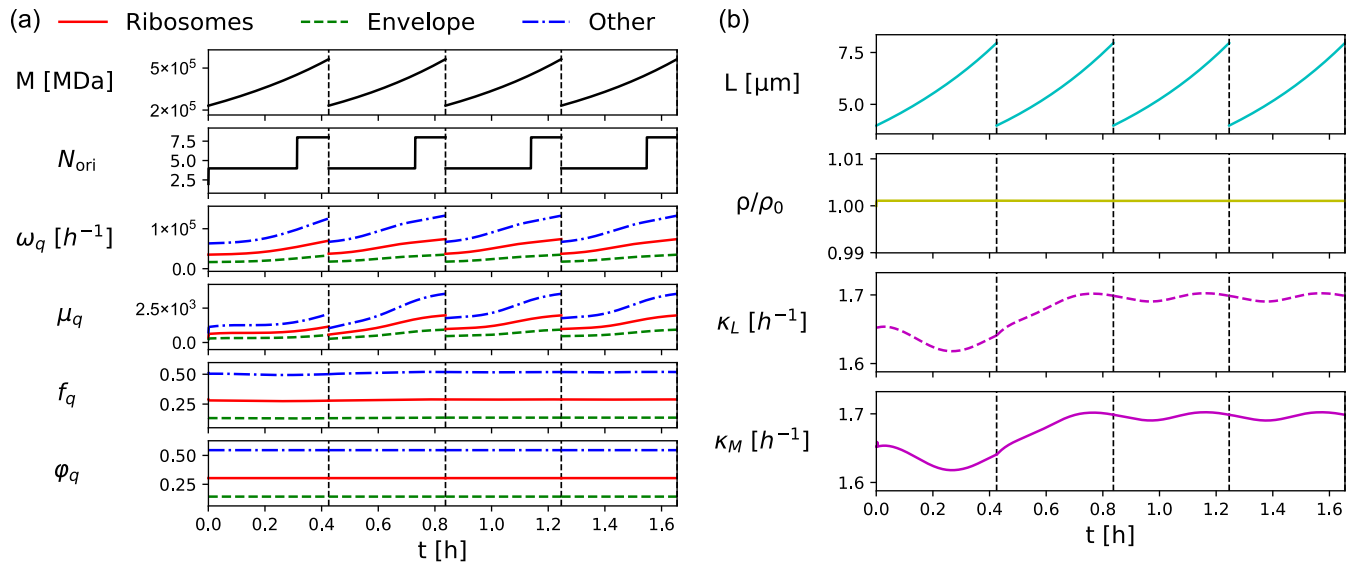

FIG. 3. Representative simulation of the DNA-proportional transcription model, showing the evolution of cell physiological variables. (a) Trajectories of physiological variables evolved in the model (top to bottom): cell mass M, the number of replication origins N_{ori}, transcription rates ω_q, mRNA abundance μ_q, proteome allocation fraction f_q, and mass fraction ϕ_q. Step increase in replication origins per cell denotes replication initiation. The dashed-vertical line denotes a cell division event. The parameters used are $\kappa_{n,0} = 25\,\text{h}^{-1}$, $\omega_R = 1.77 \times 10^4\,\text{h}^{-1}$, $\omega_E = 8.45 \times 10^3\,\text{h}^{-1}$, and $\omega_0 = 3.18 \times 10^4\,\text{h}^{-1}$ with a steady-state tolerance window of 1%. (b) Model output showing the trajectory of (top to bottom) cell length L, normalized cell density ρ/ρ_0, elongation rate κ_L, and mass growth rate κ_M for the simulation corresponding to data in (a). Density is relative to the initialized value $\rho = 1.9 \times 10^5\,\text{MDa}/\mu\text{m}^3$ [51]. Elongation and growth rates are calculated according to Eqs. (15) and (16), respectively.

state are determined entirely by the volume initiation criterion; the initial guess only affects the time it takes to reach steady state. If the initial number of origins is too high, cell divisions will outpace DNA replication events as the volume required for initiation will not be met at any point during the cell cycle. Starting with too few replication origins will initiate multiple rounds of DNA replication in quick succession as the volume criterion for the next round of DNA replication will already be met at the start of the previous round. After cell division, if all state variables (M_q, μ_q, f_q, ϕ_q, N_{ori}) match their values at the start of the previous cycle within a small tolerance (e.g., 1%), we consider the system to have reached a steady-state cycle.

In practice, we tune the three per-chromosome transcription rates (ω_R^*, ω_E^*, ω_0^*) and the maximal nutrient uptake rate $\kappa_{n,0}$ so that the steady-state cell cycle time τ, the average envelope fraction $\bar{\phi}_E$, and the mean free ribosome fraction $\bar{f}_F$ match experimental data. For *E. coli*, $\bar{\phi}_E$ typically falls between 0.058 and 0.152 depending on growth rate [52], while *B. subtilis* in rich media has $\bar{\phi}_E \approx 0.145$ regardless of growth rate [51]. The free ribosome mass fraction $\bar{f}_F$ is approximately 0.05 in exponentially growing *E. coli* [31], a value we also adopt for *B. subtilis*.

An example simulation of the DNA-proportional transcription model is shown in Fig. 3 for *B. subtilis* growing in glycerol-rich media with $\bar{\phi}_E = 0.145$, $\bar{f}_F = 0.05$, and $\tau = 0.41\,\text{h}$. Under these conditions, 4–8 replication origins are present at any given time. However, as cell division occurs, on average, less than a quarter of the way through DNA replication, the total DNA content is only ∼5 complete chromosomes at division. As the DNA content increases, the transcription rates $\omega_q(t)$ and the corresponding mRNA abundances $\mu_q(t)$ rise throughout the cell cycle [Fig. 3(a)]. However, the allocation fractions $f_q(t)$ and mass fractions $\phi_q(t)$ remain nearly constant [Fig. 3(a)]. Consequently, both the mass growth rate κ_M and elongation rate κ_L exhibit only small amplitude fluctuations (less than 0.3% from their means at steady state), leading to near-exponential growth over each cell cycle [Fig. 3(b)].

Formally, purely exponential single-cell growth would require that the DNA content and, thus, transcription rates be strictly proportional to cell mass: $\text{DNA}(t) = \text{DNA}(0)\,M(t)/M(0)$. Any departure from this proportionality introduces small oscillations in the instantaneous growth rate about the equilibrium value. Nevertheless, our results show that logistic-style replication dynamics [Eq. (12)] still yield growth that is approximately exponential. As shown in Fig. 1, however, this near-exponential growth does not match the pronounced non-exponential growth modes (linear, super-exponential, or convex) observed in several bacterial species. Additional cell cycle-dependent transcriptional regulation is therefore necessary to reproduce those distinctly non-exponential growth phenotypes.

V. ORIGINS OF NON-EXPONENTIAL GROWTH

Gene expression can vary extensively due to environmental changes [31,36] and transiently during gene duplication [42,43]. Since simple proportionality between transcription rate and DNA content fails to reproduce experimentally observed dynamics of elongation rate κ_L (compare Figs. 1 and 3), we next consider how deviations from DNA-proportional transcription [Eq. (13)] affect growth-rate dynamics. Specifically, we explore cell-cycle periodic perturbations of the transcription rates $\omega_q(t)$ that preserve steady-state growth

across generations. Physically, these perturbations could arise from changes in RNA polymerase concentration or promoter activity. Although our model does not explicitly track gene regulators, it captures how altered probabilities of transcriptional "bursting" events translate to changes in average growth rate.

In Sec. V A, we illustrate the qualitative impact of gene-expression perturbations using a square-wave perturbation to the transcription rate. Next, Sec. V B investigates how sinusoidal variations in ribosome and envelope transcription at different times and amplitudes within the cell-cycle impact growth rate. We then examine, in Sec. V C, the timescales on which these regulatory changes influence growth. Finally, Sec. VI uses these insights to elucidate the diverse non-exponential growth patterns observed in different bacterial species.

A. Deviation from DNA-proportional transcription

To understand how dynamic changes in transcription rate affect growth-rate dynamics, we first consider a simple, square-wave perturbation to the transcription rate with clearly defined "on" and "off" phases. Specifically, let

$$\begin{aligned}\omega_q(t) &= \omega_q^*[\mathrm{DNA}(t) \; + \; \beta_q(t)] \\ &= \omega_q^*\left[\mathrm{DNA}(t) \; + \; \beta\, \Pi\left(\frac{t-t_p}{\tau_p}\right)\right], \end{aligned} \tag{17}$$

where $\beta_q(t)$ is the perturbation term, Π is the Heaviside (step) function, τ_p the pulse duration, and t_p the pulse initiation time. Thus, at time t_p, transcription rate of sector q increases by an amount β for a period of length τ_p, after which it returns to the baseline $\omega_q^*\mathrm{DNA}(t)$. Figures 4(a) and 4(b) illustrate this perturbation for the ribosome sector ($\beta_R \neq 0$, $\beta_E = 0$), and Figs. 4(c) and 4(d) do so for the envelope sector ($\beta_R = 0$, $\beta_E \neq 0$).

In the case of perturbation to the transcription rate of ribosomal proteins [Figs. 4(a) and 4(b)], f_R rises during the pulse and returns to its initial level afterward. Consequently, the mass growth rate κ_M increases while the elongation rate κ_L decreases, reflecting the trade-off between ribosomal (f_R) and envelope (f_E) proteome allocation. The cell dry mass density (relative to the initial density ρ_0, $\rho/\rho_0 = M/M_E$) temporarily increases during the perturbation and remains slightly elevated on average compared to the unperturbed steady state because of the periodic nature of the perturbation. Notably, changing ω_R affects κ_M more strongly than κ_L, emphasizing the ribosomal sector's primary role in controlling mass growth rate.

By contrast, perturbations to the transcription of envelope proteins [Figs. 4(c) and 4(d)] increases f_E with minimal impact on f_R, leading to an increase in κ_L. Although the initial cycle shows a mild decrease in κ_M, this effect is partially offset by the adder-like division criterion on M_E, which triggers division at a lower total mass and lowers the overall cell density in subsequent cell cycles. Consequently, perturbing ω_E predominantly influences κ_L rather than κ_M, underscoring how envelope allocation principally drives cell elongation. In both scenarios, resource allocation constraints introduce secondary feedbacks, but the primary effect remains sector-specific: perturbing ribosome transcription mainly alters bulk mass growth, whereas envelope transcription primarily affects elongation.

B. Cyclical gene expression

Having established a basic intuition for how transcriptional fluctuations shape growth, we now introduce a biologically motivated form of time dependence of transcription rate. Since gene expression must be cell-cycle periodic at steady state, many functions could, in principle, model such oscillatory behavior. To compare scenarios where transcription changes primarily in the first versus the second half of the cycle, we use a simple sinusoidal perturbation,

$$\omega_q'(t) \; = \; \omega_q^*[\mathrm{DNA}(t) \; + \; \beta_q(1+\sin(2\pi t/\tau))], \tag{18}$$

where β_q sets the perturbation amplitude for sector q. Such periodic regulation may arise from diverse biological mechanisms, including promoter-specific regulation or feedback loops tied to replication, division, and morphogenesis [25,34]. Unlike the square-wave perturbation, this smooth, continuous function better approximates the average outcome of noisy biochemical processes.

Figure 5(a) shows an example perturbation of this form, where ω_R is increased in the first half of the cell cycle, while ω_E is increased in the second half. Correspondingly, Fig. 5(b) shows that the elongation rate κ_L decreases and the mass growth rate κ_M increases during the interval of higher ribosome expression, and vice versa for envelope expression. This leads to a local maximum in κ_M roughly at midcycle, shortly after a minimum in κ_L.

To explore these effects systematically, we map how β_R and β_E influence the range of κ_L and κ_M over each cell cycle [Figs. 5(c) and 5(d)]. As with the square-wave perturbations, changes in ω_R primarily affect κ_M, while shifts in ω_E principally alter κ_L. However, their relative phases also matter. When ribosome and envelope perturbations are out-of-phase (opposite signs for β_R and β_E), the elongation rate exhibits the largest changes, owing to trade-offs in allocation. By contrast, in-phase perturbations (same signs for β_R and β_E) yield more pronounced variations in κ_M as such perturbations result in oscillations of the total transcription rate. Here, a decrease (increase) in the total transcription rate would decrease (increase) mRNA concentration, which in turn increases (decreases) the free ribosome mass fraction leading to a decrease (increase) in the translation rate. Notably, these fluctuations differ by an order of magnitude, with κ_L fluctuations typically on the order of $10^{-1}\,\mathrm{h}^{-1}$ and κ_M fluctuations on the order of $10^{-2}\,\mathrm{h}^{-1}$. Likewise, variations in κ_L from changing ω_E generally exceed those from altering ω_R. Thus, the timing and amplitude of gene-expression oscillations can systematically reshape both mass and length growth rates.

C. Timescale of gene-expression perturbations and growth-rate response

Although time-dependent changes in gene expression lead to deviations from exponential growth, such transcriptional perturbations do not instantaneously alter growth rates.

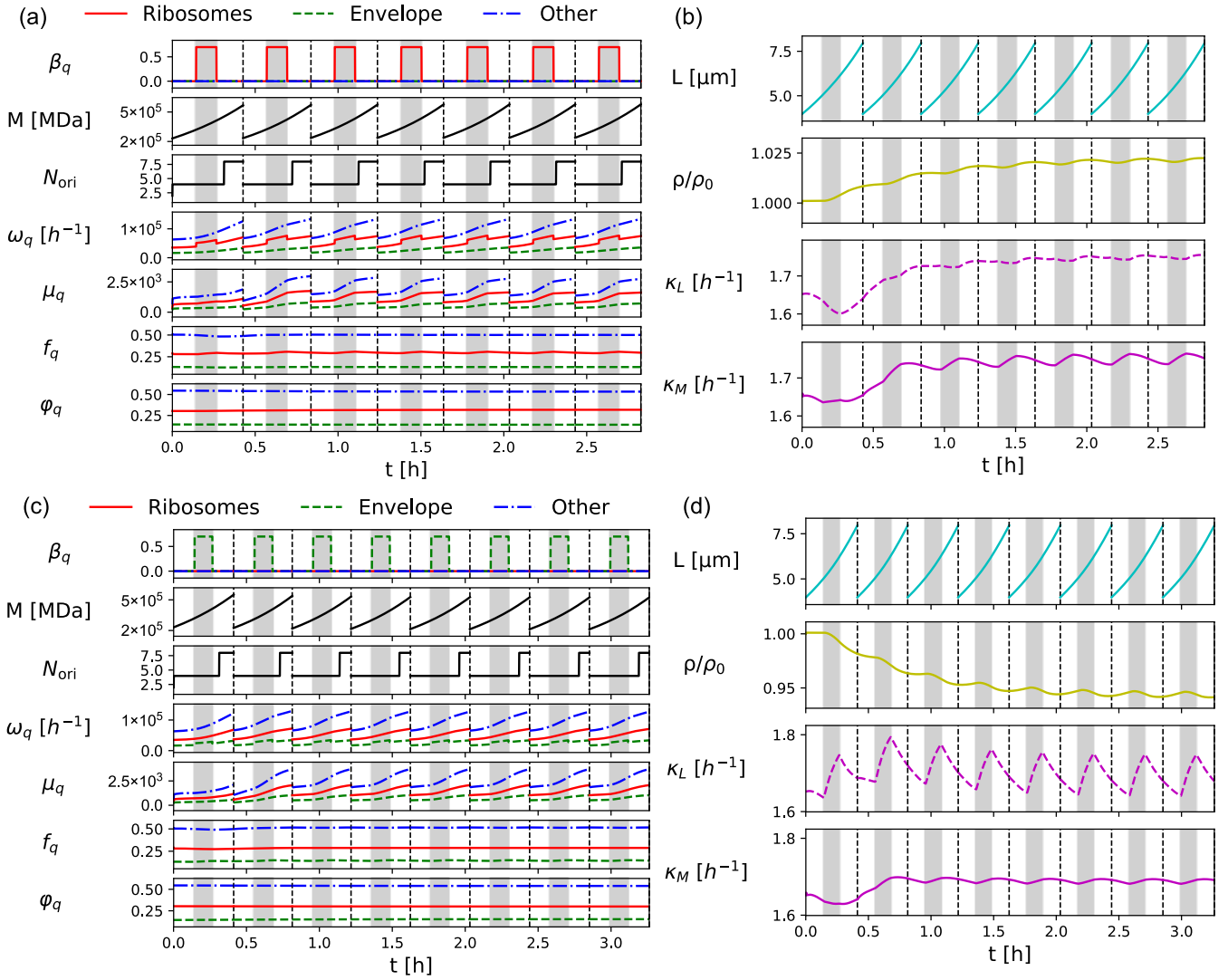

FIG. 4. Effects of transcription perturbations on cell growth. (a) Trajectories of physiological variables evolved in the model (top to bottom): perturbation to transcription rates β_q, cell mass M, the number of replication origins N_{ori}, transcription rates ω_q, mRNA abundance μ_q, proteome allocation fraction f_q and mass fraction ϕ_q. Here, we only consider a square wave perturbation to the transcription rate of ribosomal proteins in absolute time. The square wave perturbation is given by Eq. (17) with the parameters $t_p = 0.5\tau$, $\tau_p = 0.3\tau$, and $\beta = 0.7$. This period is illustrated with a grey region in each cell cycle. (b) Model output showing the trajectory of (top to bottom) cell length L, normalized cell density ρ/ρ_0, elongation rate κ_L, and mass growth rate κ_M for the simulation corresponding to data in (a). Density is relative to the initialized value $\rho = 1.9 \times 10^5$ MDa/μm^3 [51]. Elongation and growth rates are calculated according to Eqs. (15) and (16), respectively. (c) and (d) show an identical perturbation, but to the expression of cell envelope proteins ω_E rather than the cell envelope.

Instead, they must propagate through multiple molecular layers before manifesting in observable changes to mass or elongation rates. We thus elucidate how quickly (or slowly) these perturbations translate into changes in elongation (κ_L) and mass growth (κ_M) rates. Our simulations reveal stark contrasts: Transcriptional changes typically take hours to manifest in our coarse-grained sectors, whereas proteome allocation shifts can elicit immediate responses.

To illustrate this, consider a step-function decrease in ω_R [Fig. 6(a)]. Even though ribosomal transcription declines abruptly, the effect on κ_M takes several hours, as the altered ribosome production must propagate through both the transcriptome and proteome. Meanwhile, κ_L temporarily increases owing to a relative boost in envelope expression, but it too settles to the new steady state only after around four hours. A similar step decrease in ω_E [Fig. 6(b)] triggers an immediate reduction in κ_M, while κ_L first falls to a minimum, then ramps back up over a comparable timescale.

In contrast, altering proteome allocation fractions f_q produces rapid shifts in growth rates [Figs. 6(c) and 6(d)]. A sudden drop in f_R (with f_F rising accordingly) instantly lowers κ_M and boosts κ_L, since a larger fraction of ribosomes is devoted to envelope synthesis. This transient peak in κ_L emerges in half the time required for the transcriptional perturbation, and the system then returns to the original steady state. Likewise, reducing f_E prompts an immediate decrease in both κ_L and κ_M, followed by an overshoot and a return to equilibrium within roughly half an hour.

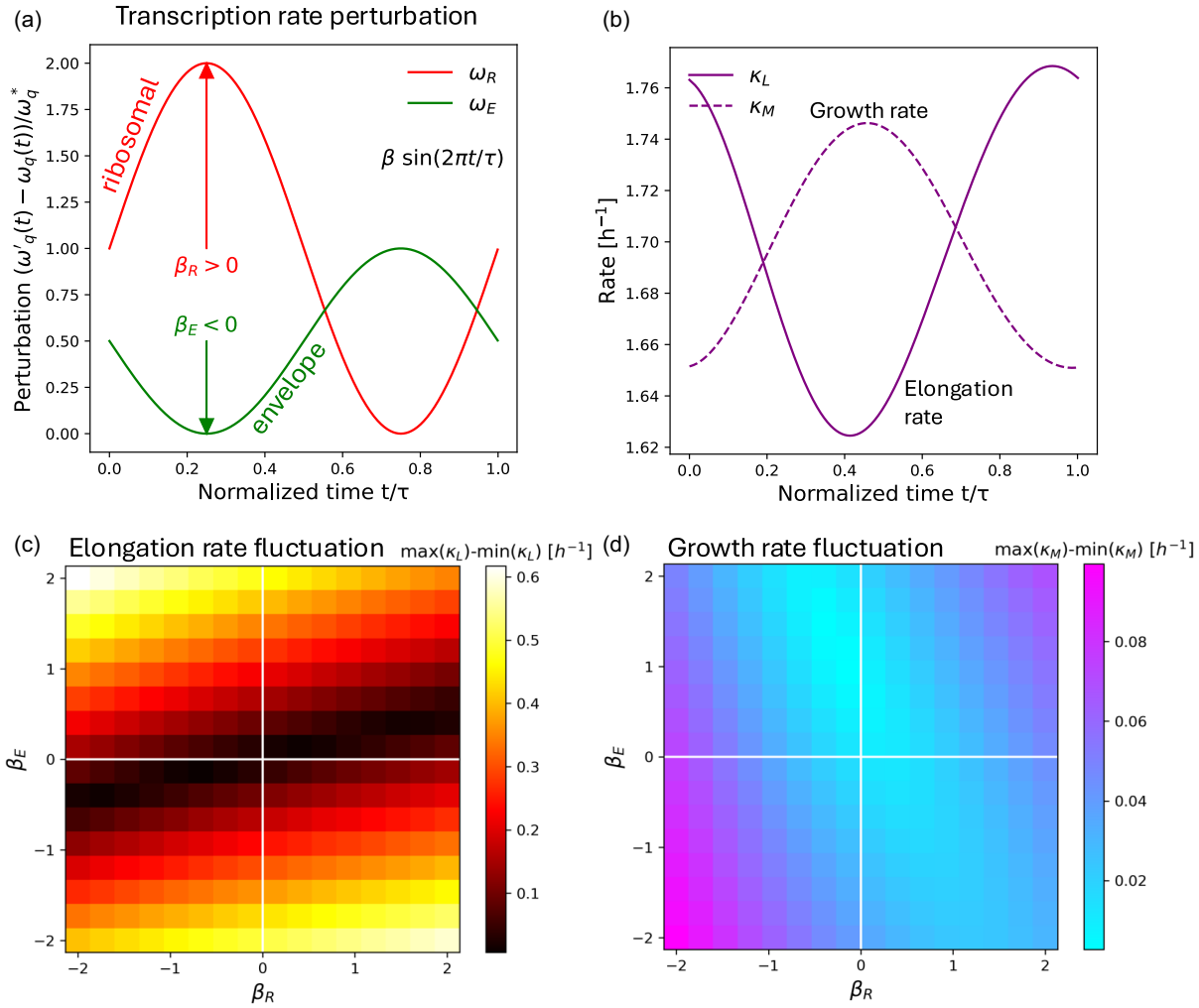

FIG. 5. Effects of cyclical gene expression on growth. (a) A representative set of sinusoidal perturbations to $\omega_R(t)$ and $\omega_E(t)$ as defined in Eq. (18) plotted against normalized time t/τ, where τ is cell-cycle duration. Note that the sign of β determines whether or not the phase is offset by π. (b) Elongation and growth rates corresponding to the perturbation in (a) applied to the cell simulated in Fig. 3: $\kappa_{n,0} = 25\,\mathrm{h}^{-1}$, $\omega_R = 1.77 \times 10^4\,\mathrm{h}^{-1}$, $\omega_E = 8.45 \times 10^3\,\mathrm{h}^{-1}$, and $\omega_0 = 3.18 \times 10^4\,\mathrm{h}^{-1}$ with a steady-state tolerance of 1%. (c) A colormap showing the range of the elongation rate during the cell cycle. The y axis corresponds to the magnitude ($|\beta|$) and phase (sign of β) of the envelope perturbation and the x axis corresponds to the ribosomal transcription perturbation. The white lines denote the quadrants in which the perturbations are either in or out of phase with each other. Cell-cycle averaged mass fractions and cell cycle time are constrained to be the same as the unperturbed state for each entry by fitting ω_R, ω_E, and ω_0. (d) A colormap showing the range of the mass growth rate during the cell cycle with the same axes as (c).

Thus transcriptional regulation operates on hours-long timescales, reflecting the need for new mRNA transcripts and protein turnover. By contrast, direct changes to proteome allocation fractions can rewire growth rates almost instantaneously. This disparity highlights the multilayered nature of bacterial growth control, wherein slower upstream processes (transcription) and faster downstream processes (allocation) together shape the overall dynamics of cell growth.

VI. MODELING NON-EXPONENTIAL ELONGATION MODES IN BACTERIAL CELLS

A. Convex growth of *B. subtilis*

The periodic transcription perturbations described in Sec. V B provide a framework for understanding the convex growth pattern of *Bacillus subtilis*. Experimentally, the elongation rate of *B. subtilis* has been observed to change by $0.18\,\mathrm{h}^{-1}$ to $0.52\,\mathrm{h}^{-1}$ across the cell cycle [8]. From Fig. 5, we see that achieving such a substantial temporal variation in κ_L requires a pronounced, cell-cycle-dependent increase in envelope transcription ω_E. Whether or not ribosome transcription ω_R must also vary remains to be seen; however, the data strongly suggest that growth-related envelope genes do not remain at a fixed transcription level throughout the cycle.

To quantitatively understand the behavior of ω_R, we fit a sinusoidal perturbation [generalized from Eq. (18) to include a phase shift] to the ensemble-averaged elongation rate data in Fig. 1(b),

$$\omega_q(t) = \omega_q^* \left[\mathrm{DNA}(t) + \beta_q \left(1 + \sin\left(2\pi \left(\frac{t}{\tau} - \theta_q \right) \right) \right) \right], \tag{19}$$

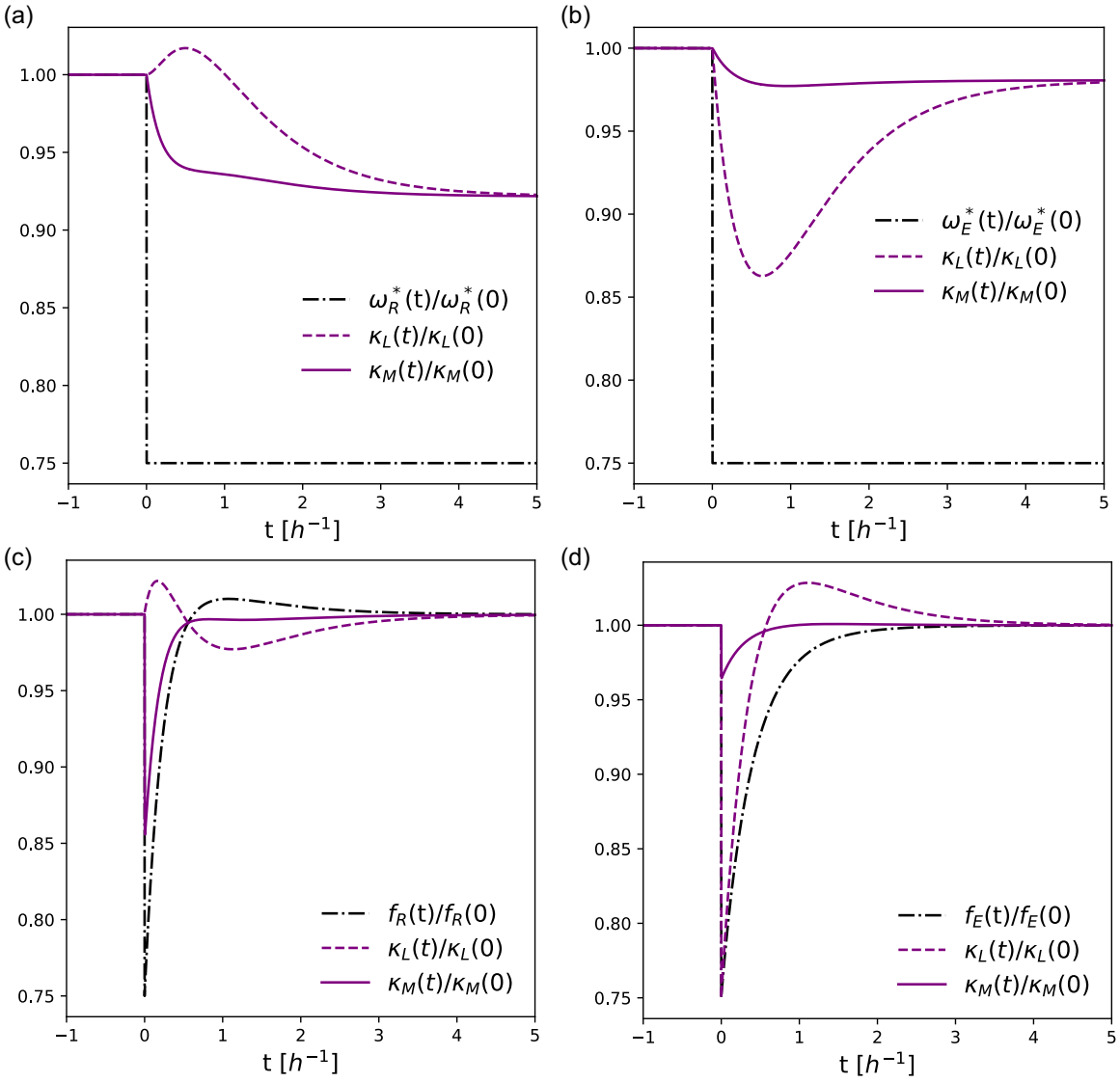

FIG. 6. Timescale limitations of the effects of gene expression on growth. (a) A simulation of balanced exponential growth with $\omega(t)$ determined by Eq. (13). At $t = 0$, ω_R^* is decreased to $0.75\omega_R^*$. We plot the effects of this transcription perturbation on elongation and growth rates, as calculated by Eqs. (15) and (16). (b) Considers an identical scenario to (a) except with a step decrease in ω_E^*. (c) Simulating the effects of a step decrease in f_R by a factor of 0.75, on cell growth and elongation rates. Note that f_R relaxes back to the initial value as ω_R remains unchanged. (d) Shows the effects of a step decrease in f_E.

where the parameter θ_q sets the phase. Figure 7(a) shows an example fit of this form. We see that, as expected, there is an increase in ω_E during the later half of the cell cycle when κ_L increases in the data [Figs. 7(c) and 7(d)]. The fit also indicates a corresponding trade-off in ω_R; rather than adjusting ω_E alone, ribosome transcription is front-loaded in the cycle while envelope transcription is back-loaded. As seen previously in Fig. 5(c), these out-of-phase perturbations drive changes in κ_L without altering the cell's average mass fractions or cycle time.

As ribosomal genes are typically located near the replication origin [53], it is expected for $\omega_R(t)$ to increase shortly after DNA replication as there is a relative increase in ribosomal gene dosage. As seen in Fig. 7(b), we do see an increase soon after DNA replication as expected, and we see a maximum $\omega_R(t)$ around halfway through DNA replication. A more flexible fitting function—one that allows the minima and maxima to be optimized directly—could capture this maximum with greater precision, but doing so would require additional free parameters and would compromise the simplicity, predictive character of our current model.

Interestingly, despite both ω_R and ω_E being perturbed, κ_M remains nearly constant compared to the pronounced midcycle dip and rise in κ_L. This implies that the experimentally observed convex elongation rate profile does not reflect significant changes in the overall mass growth rate. Instead, the envelope-specific transcription dynamics cause minor cyclic fluctuations in the cell's dry mass density, producing a convex elongation pattern in real time. This distinction underscores how subtle variations in sector-specific gene expression can manifest as noticeable cell-shape changes, even when total biomass growth remains close to exponential.

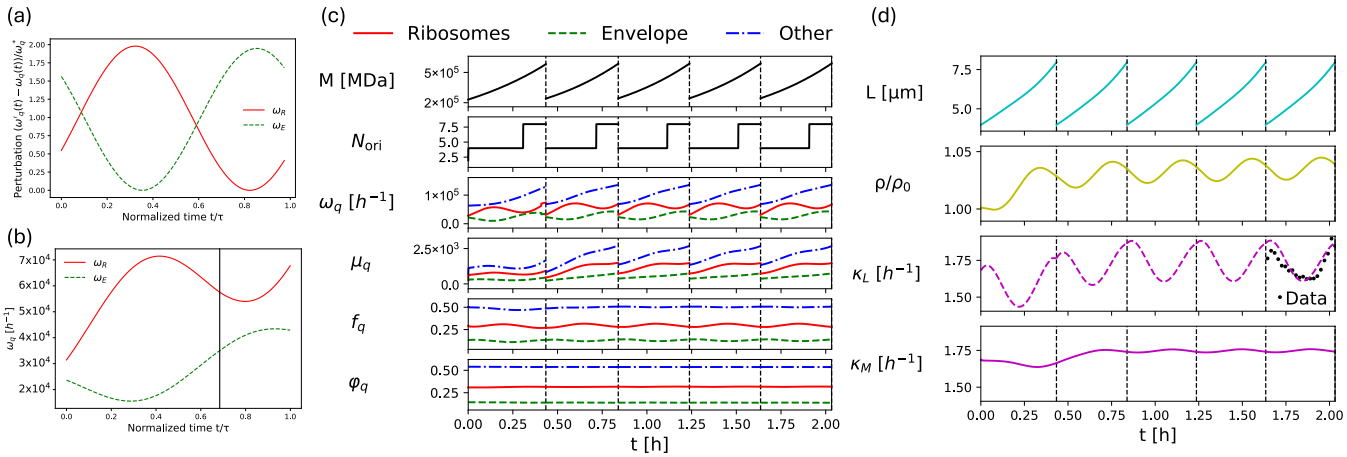

FIG. 7. Modeling convex elongation rate profile of *B. subtilis*. (a) Perturbations to ribosome and cell envelope transcription rates, of the form in Eq. (19), plotted against normalized time t/τ, where τ is cell cycle duration. The perturbation profile is fitted to the elongation rate data of *B. subtilis* cells [see (c)]. Fitting parameters are $\beta_R = 0.99$, $\beta_E = 0.97$, $\theta_R = 0.93$ h, and $\theta_E = 0.40$ h. (b) Trajectories of the cell physiological variables predicted by model simulation, corresponding to the perturbations shown in (a). The parameters used are $\kappa_{n,0} = 25\,\mathrm{h}^{-1}$, $\omega_R = 1.77 \times 10^4\,\mathrm{h}^{-1}$, $\omega_E = 8.45 \times 10^3\,\mathrm{h}^{-1}$, and $\omega_0 = 3.18 \times 10^4\,\mathrm{h}^{-1}$. (c) Simulation outputs for cell length, density, elongation rate and growth rate for the simulation results presented in (b). Density is relative to the initialized value $\rho = 1.9 \times 10^5\,\mathrm{MDa/\mu m^3}$ [51]. Elongation and growth rates are calculated according to Eqs. (15) and (16), respectively. Elongation rate data are for *B. subtilis* BSB1 cells grown in Glycerol at 37 °C [8].

B. Super- and subexponential growth

Both super-exponential and linear growth exhibit a jump discontinuity at division [Fig. 1(a)] as, on average, the elongation rate resets to its value at the start of the previous cell cycle. In Sec. V C, we showed that an instantaneous change in gene expression at division cannot, by itself, generate this instantaneous shift in elongation rate on the short (∼1 minute) timescale. Given that cell division is symmetric on average for *E. coli* [4], the only remaining mechanism is a change in proteome allocation fractions due to division itself.

Focusing on the monotonic changes in elongation rate observed in super-exponential and linear growth, suppose that the simplest possible time dependence in proteome allocation fractions is a linear increase (or decrease) throughout the cell cycle, followed by a jump discontinuity at division. In that case, we can write

$$f_q(t) = \bar{\phi}_q + \Delta_q\left(\frac{t}{\tau} - \frac{1}{2}\right), \tag{20}$$

where $\bar{\phi}_q$ is the cycle-averaged mass fraction, τ is the cell cycle time, and Δ_q is the overall change in f_q over one cycle. Fitting Eq. (20) to *E. coli* data [4] [Figs. 8(a) and 8(b)] shows that f_E grows throughout the cell cycle and then returns to its initial value at the next generation, mirroring a previous super-exponential growth model [27]. By contrast, fitting the same form to *M. tuberculosis* data [42] implies a decrease in envelope allocation (f_E) over the cell cycle—indicating that superexponential growth arises from a relative increase in allocation to ribosomes, whereas linear growth is driven by a relative decrease.

Figure 8(c) illustrates how the change in κ_L from birth to division depends on Δ_R and Δ_E. Positive Δ_E leads to super-exponential growth, negative Δ_E to sub-exponential growth (with linear growth as a special case). Once Δ_E is fixed, Δ_R has minimal effect on the overall change in κ_L, meaning that changes in f_E primarily drive growth on the timescale of a single cell cycle. However, Δ_R does influence the concavity of the κ_L trajectory, yielding slight non-monotonic regions if Δ_R is large compared to Δ_E. Figure 8(f) shows that these non-monotonic deviations remain small and do not produce full oscillations, agreeing with our discussion in Sec. V B. Thus, Δ_E sets the amplitude of the κ_L variation, while Δ_R determines whether the curve is concave or convex. When $\Delta_R > 0$, the trajectory is convex, in contrast to the concave shape shown in Fig. 8(b) for $\Delta_R \leqslant 0$. Since super-exponential growth in filamentous *E. coli* is known to approach exponential growth asymptotically [27] (i.e., a concave shape), our model supports the scenario of $\Delta_R \leqslant 0$. In short, we predict a trade-off in proteome allocation: ribosome synthesis is prioritized early in the cycle, while envelope synthesis is prioritized later.

Returning to the full gene expression-driven model, Figs. 6(c) and 6(d) show that a step-like change to f_R or f_E (e.g., at division) without transcriptional adjustments simply relaxes back to steady state on the same timescale that filamentous cells reach steady-state growth [27]. This indicates that time-dependent gene expression is not strictly necessary to produce super-exponential growth; a division-based reallocation alone can suffice. In addition, the localization of cell envelope growth can inform the full gene expression-driven model. As the end caps of *E. coli* do not grow [54], transcription of the envelope sector must increase throughout the cell cycle as the growing surface area fraction increases. In contrast, *M. tuberculosis* only grows at the poles [42] so the relative transcription rate in the envelope sector must decrease as the growing surface area fraction decreases. These underlying features contribute to the ribosome allocation dynamics seen in Figs. 8(a) and 8(d).

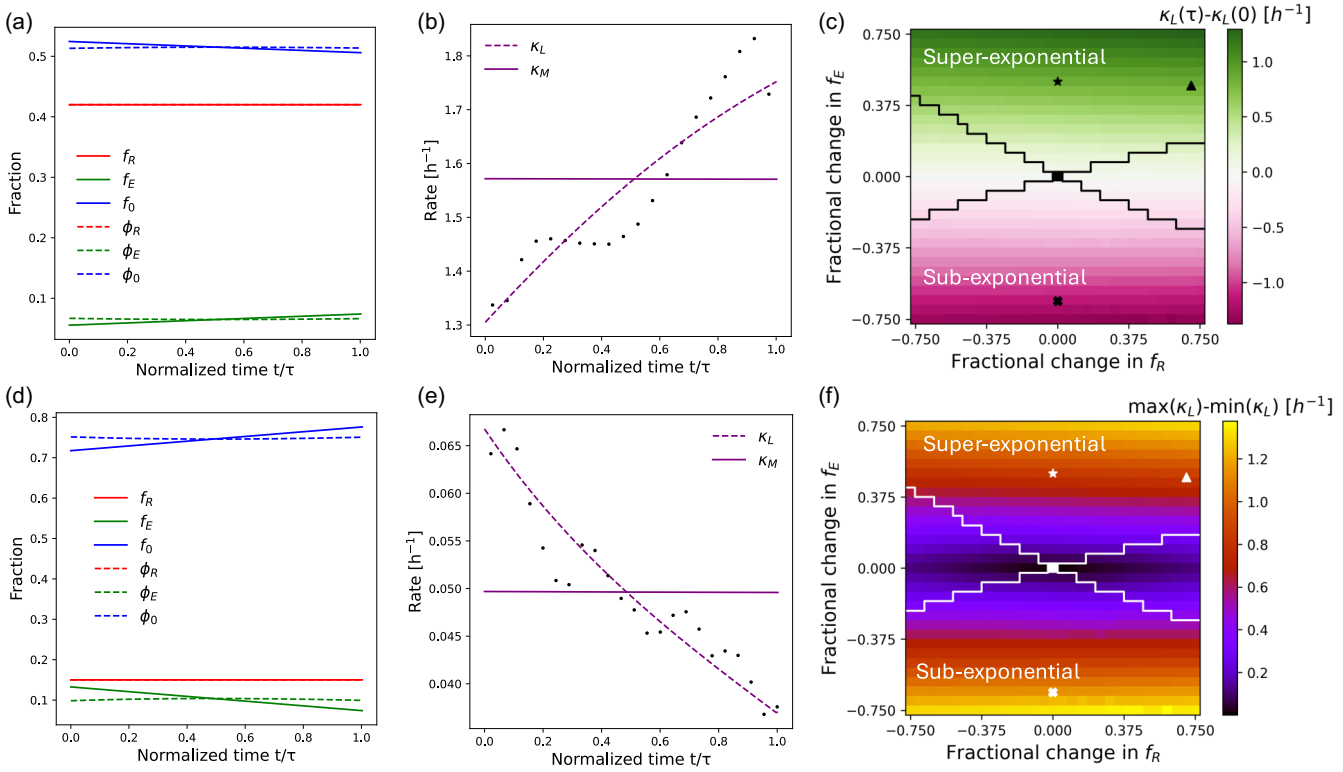

FIG. 8. Dynamic resource allocation during super- and sub-exponential elongation. (a) Proteome allocation fractions [solid lines, Eq. (20)] and integrated mass fractions (dashed lines) vs normalized time t/τ, fitted to *E. coli* super-exponential growth rate data [4]. The fitted parameter values are: $\Delta f_E = 0.037$, $\kappa_t = 3.74\,\mathrm{h}^{-1}$, $\bar{\phi}_E = 0.074$, $\bar{\phi}_R = 0.22$ [31]. (b) Elongation [Eq. (15)] and mass growth rates (Eq. (16)) corresponding to the allocation in (a), plotted against normalized time t/τ. The plotted points show the ensemble-averaged growth rate data for *E. coli* K12 NCM3722 cells, grown in supplemented Glucose media at 37 °C [4]. (c) Heatmap of the net change in elongation rate from birth ($t = 0$) to division ($t = \tau$), varying the fractional changes in envelope (Δf_E) and ribosome (Δf_R) allocation. The diagonal line divides super-exponential (top) and sub-exponential (bottom) regimes; left and right regions denote monotonic vs non-monotonic growth. The star marks the *E. coli* fit in (a), (b), the triangle marks a variant with ($\Delta f_R = 0.18$, $\bar{\phi}_R = 0.26$, $\Delta f_E = 0.035$, $\bar{\phi}_E = 0.074$), the cross marks the linear fit in (d), (e), and the black square at the origin denotes purely exponential growth. (d) Analogous resource allocation fit for *M. tuberculosis* ($\Delta f_E = -0.12$, $\kappa_t = 0.33\,\mathrm{h}^{-1}$, $\bar{\phi}_R = 0.15$, $\bar{\phi}_E = 0.074$). (e) Corresponding elongation and mass growth rates, plotted with *M. tuberculosis* data [30]. (f) Heatmap of the total range of elongation rate over one cycle, labeled as in (c).

VII. DISCUSSION

Recent single-cell measurements reveal that bacterial elongation diverges from the standard assumption of exponential growth, instead showing convex, super-exponential, or sub-exponential elongation rate profiles across species. To explain these patterns, we built a minimal mechanistic model linking transcription and proteome allocation to overall mass growth and elongation rate. Under the simplest assumption of mRNA synthesis rate proportional to gene dosage, the model predicts near-exponential growth in cell size and mass—which fails to capture the observed modes of elongation rates in single-cell data. Consequently, we explored how deviations from DNA-proportional transcription could shape growth dynamics.

In particular, we introduced cell-cycle periodic perturbations to transcription and analyzed their effects. Altering ribosome expression strongly influences mass growth rate, while envelope expression modulations most profoundly affect elongation rate. When total transcription shifts in-phase, mass growth changes significantly; however, out-of-phase peaks in ribosome and envelope expression lead to more dramatic fluctuations in elongation. Crucially, envelope-specific perturbations shift elongation by roughly an order of magnitude more than ribosomal changes do. Fitting our model to *B. subtilis* data shows that convex elongation rate requires envelope allocation to change over the cell cycle, balanced by a trade-off with ribosome synthesis.

We next turned to how some species achieve super-exponential or sub-exponential growth with apparent jump discontinuities at division. Our analysis shows that instantaneous changes in gene expression alone cannot produce such sharp transitions. Instead, a division-induced shift in resource allocation is required, resetting envelope synthesis at each division event. Super-exponential growth follows when envelope allocation increases throughout the cycle but dips at division, whereas sub-exponential growth occurs when envelope allocation decreases over the cycle and then rebounds at division. This mechanism aligns with observations in *E. coli*, where non-growing poles reduce the actively elongating surface area immediately post-division, which subsequently expands as cells elongate. The growing region of the envelope and resource allocation are interchangeable ways of thinking about the system; an increase in the fraction of growing surface area permits increases the fraction of resources

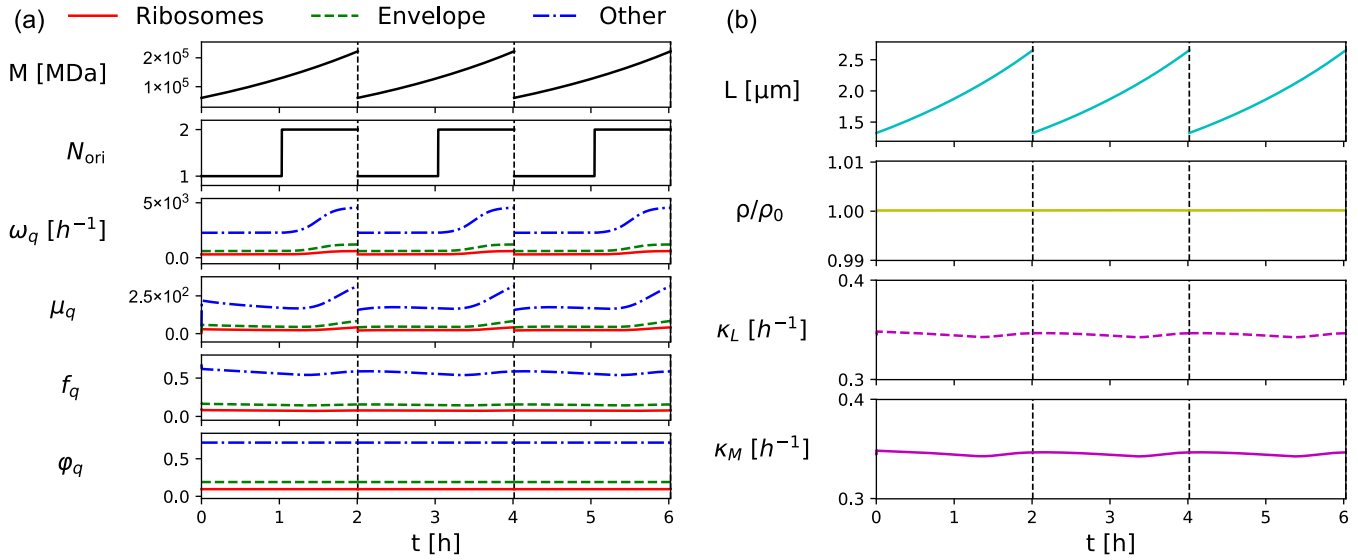

FIG. 9. Representative simulation of the DNA-proportional transcription model in minimal media. (a) Trajectories of physiological variables evolved in the model (top to bottom): cell mass M, the number of replication origins N_{ori}, transcription rates ω_q, mRNA abundance μ_q, proteome allocation fraction f_q, and mass fraction ϕ_q. Step increase in replication origins per cell denotes replication initiation. The dashed-vertical line denotes a cell division event. The parameters used are $\kappa_{n,0} = 2\,\text{h}^{-1}$, $\omega_R = 3.02 \times 10^2\,\text{h}^{-1}$, $\omega_E = 6.03 \times 10^2\,\text{h}^{-1}$, and $\omega_0 = 2.27 \times 10^3\,\text{h}^{-1}$ with a steady-state tolerance window of 1%. (b) Model output showing the trajectory of (top to bottom) cell length L, normalized cell density ρ/ρ_0, elongation rate κ_L, and mass growth rate κ_M for the simulation corresponding to data in (a). Density is relative to the initialized value $\rho = 1.9 \times 10^5\,\text{MDa}/\mu\text{m}^3$ [51]. Elongation and growth rates are calculated according to Eqs. (15) and (16), respectively.

allocated towards envelope growth and vice versa. In contrast, *M. tuberculosis*—which elongates only from its poles—shows a surge in envelope allocation upon activating new poles after division, then tapers as the cell elongates. As the growing region of the envelope is fixed during the cell cycle, the fraction of resources allocated to elongation can only decrease with time, in agreement with our model.

While our model captures the core aspects of cell-cycle-dependent growth rate profiles, it does not predict a unique transcription-time profile from elongation data alone. Future experiments quantifying single-cell transcription, dry mass density, and translational activity (e.g., via ribosome profiling) could refine these predictions. Additionally, we employ a minimal proteome perspective, omitting detailed functions of complexes such as the elongasome or divisome and ignoring potential noise in transcription or division timing. Still, our findings highlight how non-exponential elongation can emerge from coordinated changes in envelope and ribosome expression, coupled with division-driven resource reallocation. Ultimately, the evolutionary or fitness benefits of non-exponential elongation remain unclear, since deviations from balanced, exponential growth appear to exert only minor effects on cell cycle timing. Nonetheless, understanding why cells deviate from perfectly exponential growth, even when balanced biosynthesis seems optimal, can reveal intra-generational physiological strategies that remain hidden in population-averaged data.

ACKNOWLEDGMENTS

This work is supported by the National Institutes of Health (NIH R35 GM143042) and the Shurl and Kay Curci Foundation.

DATA AVAILABILITY

The data that support the findings of this article are publicly available [55].

APPENDIX A: GROWTH IN MINIMAL MEDIA

The representative simulation shown in Sec. IV (Fig. 3) illustrates a fast growth condition. It is not immediately obvious that the same conclusions hold for slow growth conditions or in minimal media. Most importantly, the cell cycle duration in Fig. 3 is less than the C period of DNA replication, while in slower growth conditions the doubling time may exceed the C period by a large margin. In such a condition, our assumption of transcription rate proportional to DNA content may be less applicable if transcription is limited by RNAP concentration (or other factors) rather than DNA concentration. To test the relevance of our model to these slower growing cells, we simulated a doubling time on the order of 2 hours—the approximate growth rate of *B. subtilis* in minimal media [56]—with only one chromosome per cell in Fig. 9. Here, we see that increases in transcription rates are localized to DNA replication rather than increasing gradually throughout the cell cycle. However, cells are still capable of remaining within ∼1% deviations from exponential elongation and mass growth. Thus, our model assumptions still predict near-exponential growth in slow-growth conditions.

APPENDIX B: CHANGES IN DRY MASS DENSITY

Recent experiments have shown that *E. coli* exhibits a ∼6% dip in dry mass density midway through the cell cycle, relative to its value at division [20]. This observation places

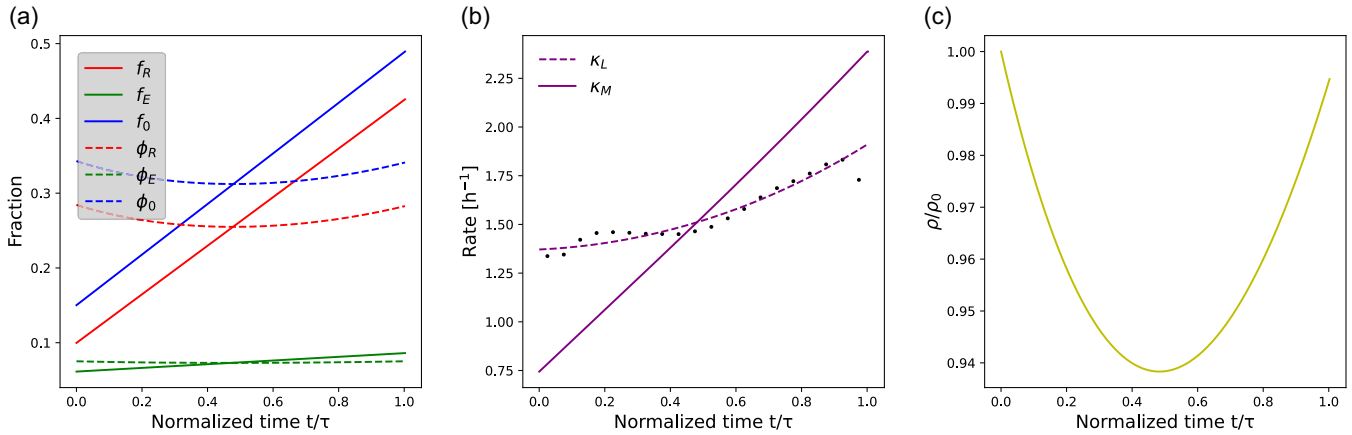

FIG. 10. Changes in dry mass density in *E. coli*. (a) Ribosome allocation fractions [solid lines, Eq. (20)] and integrated mass fractions (dashed lines) vs normalized time t/τ, fitted to *E. coli* super-exponential growth rate data [4]. The fitted parameter values are: $\Delta f_E = 0.025$, $\bar{\phi}_E = 0.074$, $\Delta f_R = 0.32$, $\bar{\phi}_R = 0.21$, $\Delta f_0 = 0.32$, and $\bar{\phi}_0 = 0.24$ with $\kappa_t = 5.9\,\mathrm{h}^{-1}$. (b) Elongation [Eq. (15)] and mass growth rates [Eq. (16)] corresponding to the allocation in (a), plotted against normalized time t/τ. The plotted points show the ensemble-averaged growth rate data for *E. coli* K12 NCM3722 cells, grown in supplemented Glucose media at 37 °C [4]. (c) Normalized cell dry mass density corresponding to the resource allocation strategies shown in (a).

additional constraints on the minimal model for super-exponential growth described in Sec. VI B. For density to decrease during the cycle, the mass growth rate κ_M must fall below the elongation rate κ_L, and vice versa. The model presented in Figs. 8(a) and 8(b) does not reproduce the expected density dynamics; the mass growth rate is smaller (larger) than the elongation rate for the first (second) half of the cell cycle, implying a density maximum in the middle of the cell cycle rather than at division. To have a non-constant κ_M, the translation rate must be time dependent. As discussed in Sec. V C, changes in proteome allocation alone (e.g., varying f_R) are insufficient to cause appreciable changes in κ_M on the timescale of one cycle. Instead, the mass fraction of actively translating ribosomes must be dynamic. In Fig. 10, we modify the model by allowing the total non-envelope ribosome allocation fraction to vary, relaxing the constraint $\Delta f_R + \Delta f_E + \Delta f_0 = 0$ in favor of $\Delta f_0 = \Delta f_R$. This allows the free ribosome fraction to change over time. As shown in Fig. 10(c), this adjustment yields the expected density dip during midcycle. This corresponds to a decrease in the fraction of actively translating ribosomes surrounding division, as previously suggested as a mechanism for super-exponential elongation [27]. This variation in free ribosomes represents an additional decision-making process beyond the requirements for super-exponential elongation.

[1] J. Monod, The growth of bacterial cultures, Annu. Rev. Microbiol. **3**, 371 (1949).
[2] P. Wang, L. Robert, J. Pelletier, W. L. Dang, F. Taddei, A. Wright, and S. Jun, Robust growth of *Escherichia coli*, Curr. Biol. **20**, 1099 (2010).
[3] Y. Lin, S. Crosson, and N. F. Scherer, Single-gene tuning of caulobacter cell cycle period and noise, swarming motility, and surface adhesion, Mol. Syst. Biol. **6**, 445 (2010).
[4] S. Taheri-Araghi, S. Bradde, J. T. Sauls, N. S. Hill, P. A. Levin, J. Paulsson, M. Vergassola, and S. Jun, Cell-size control and homeostasis in bacteria, Curr. Biol. **25**, 385 (2015).
[5] C. S. Wright, S. Banerjee, S. Iyer-Biswas, S. Crosson, A. R. Dinner, and N. F. Scherer, Intergenerational continuity of cell shape dynamics in *Caulobacter crescentus*, Sci. Rep. **5**, 9155 (2015).
[6] Y. Tanouchi, A. Pai, H. Park, S. Huang, N. E. Buchler, and L. You, Long-term growth data of *Escherichia coli* at a single-cell level, Sci. Data **4**, 170036 (2017).
[7] L. Susman, M. Kohram, H. Vashistha, J. T. Nechleba, H. Salman, and N. Brenner, Individuality and slow dynamics in bacterial growth homeostasis, Proc. Natl. Acad. Sci. USA **115**, E5679 (2018).
[8] J. T. Sauls, S. E. Cox, Q. Do, V. Castillo, Z. Ghulam-Jelani, and S. Jun, Control of *Bacillus subtilis* replication initiation during physiological transitions and perturbations, mBio **10**, 10.1128/mbio.02205-19 (2019).
[9] A. Amir, Cell size regulation in bacteria, Phys. Rev. Lett. **112**, 208102 (2014).
[10] M. Campos, I. Surovtsev, S. Kato, A. Paintdakhi, B. Beltran, S. Ebmeier, and C. Jacobs-Wagner, A constant size extension drives bacterial cell size homeostasis, Cell **159**, 1433 (2014).
[11] S. Jun and S. Taheri-Araghi, Cell-size maintenance: Universal strategy revealed, Trends Microbiol. **23**, 4 (2015).
[12] S. Banerjee, K. Lo, M. K. Daddysman, A. Selewa, T. Kuntz, A. R. Dinner, and N. F. Scherer, Biphasic growth dynamics control cell division in *Caulobacter crescentus*, Nat. Microbio. **2**, 17116 (2017).
[13] S. Jun, F. Si, R. Pugatch, and M. Scott, Fundamental principles in bacterial physiology—History, recent progress, and the future with focus on cell size control: A review, Rep. Prog. Phys. **81**, 056601 (2018).
[14] F. Si, G. Le Treut, J. T. Sauls, S. Vadia, P. A. Levin, and S. Jun, Mechanistic origin of cell-size control and homeostasis in bacteria, Curr. Biol. **29**, 1760 (2019).

[15] F. Si, D. Li, S. E. Cox, J. T. Sauls, O. Azizi, C. Sou, A. B. Schwartz, M. J. Erickstad, Y. Jun, X. Li *et al.*, Invariance of initiation mass and predictability of cell size in *Escherichia coli*, Curr. Biol. **27**, 1278 (2017).

[16] H. Zheng, Y. Bai, M. Jiang, T. A. Tokuyasu, X. Huang, F. Zhong, Y. Wu, X. Fu, N. Kleckner, T. Hwa *et al.*, General quantitative relations linking cell growth and the cell cycle in *Escherichia coli*, Nat. Microbiol. **5**, 995 (2020).

[17] D. Serbanescu, N. Ojkic, and S. Banerjee, Cellular resource allocation strategies for cell size and shape control in bacteria, FEBS J. **289**, 7891 (2022).

[18] L. K. Harris and J. A. Theriot, Relative rates of surface and volume synthesis set bacterial cell size, Cell **165**, 1479 (2016).

[19] N. Ojkic, D. Serbanescu, and S. Banerjee, Surface-to-volume scaling and aspect ratio preservation in rod-shaped bacteria, eLife **8**, e47033 (2019).

[20] E. R. Oldewurtel, Y. Kitahara, and S. van Teeffelen, Robust surface-to-mass coupling and turgor-dependent cell width determine bacterial dry-mass density, Proc. Natl. Acad. Sci. USA **118**, e2021416118 (2021).

[21] S. Banerjee, K. Lo, N. Ojkic, R. Stephens, N. F. Scherer, and A. R. Dinner, Mechanical feedback promotes bacterial adaptation to antibiotics, Nat. Phys. **17**, 403 (2021).

[22] J. Nguyen, V. Fernandez, S. Pontrelli, U. Sauer, M. Ackermann, and R. Stocker, A distinct growth physiology enhances bacterial growth under rapid nutrient fluctuations, Nat. Commun. **12**, 3662 (2021).

[23] M. Panlilio, J. Grilli, G. Tallarico, I. Iuliani, B. Sclavi, P. Cicuta, and M. C. Lagomarsino, Threshold accumulation of a constitutive protein explains *E. coli* cell-division behavior in nutrient upshifts, Proc. Natl. Acad. Sci. USA **118**, e2016391118 (2021).

[24] S. Bakshi, E. Leoncini, C. Baker, S. J. Cañas-Duarte, B. Okumus, and J. Paulsson, Tracking bacterial lineages in complex and dynamic environments with applications for growth control and persistence, Nat. Microbiol. **6**, 783 (2021).

[25] J. Kratz and S. Banerjee, Dynamic proteome trade-offs regulate bacterial cell size and growth in fluctuating nutrient environments, Commun. Biol. **6**, 486 (2023).

[26] P. Kar, S. Tiruvadi-Krishnan, J. Männik, J. Männik, and A. Amir, Distinguishing different modes of growth using single-cell data, eLife **10**, e72565 (2021).

[27] A. Cylke and S. Banerjee, Super-exponential growth and stochastic size dynamics in rod-like bacteria, Biophys. J. **122**, 1254 (2023).

[28] T. W. Ng, N. Ojkic, D. Serbanescu, and S. Banerjee, Differential growth regulates asymmetric size partitioning in caulobacter crescentus, Life Sci. Alliance **7** (2024).

[29] N. Nordholt, J. H. van Heerden, and F. J. Bruggeman, Biphasic cell-size and growth-rate homeostasis by single *Bacillus subtilis* cells, Curr. Biol. **30**, 2238 (2020).

[30] E. S. Chung, P. Kar, M. Kamkaew, A. Amir, and B. B. Aldridge, Single-cell imaging of the mycobacterium tuberculosis cell cycle reveals linear and heterogenous growth, Nat. Microbiol. **9**, 3332 (2024).

[31] M. Scott, C. W. Gunderson, E. M. Mateescu, Z. Zhang, and T. Hwa, Interdependence of cell growth and gene expression: Origins and consequences, Science **330**, 1099 (2010).

[32] M. Scott, S. Klumpp, E. M. Mateescu, and T. Hwa, Emergence of robust growth laws from optimal regulation of ribosome synthesis, Mol. Syst. Biol. **10**, 747 (2014).

[33] S. Hui, J. M. Silverman, S. S. Chen, D. W. Erickson, M. Basan, J. Wang, T. Hwa, and J. R. Williamson, Quantitative proteomic analysis reveals a simple strategy of global resource allocation in bacteria, Mol. Syst. Biol. **11**, 784 (2015).

[34] A. Y. Weiße, D. A. Oyarzún, V. Danos, and P. S. Swain, Mechanistic links between cellular trade-offs, gene expression, and growth, Proc. Natl. Acad. Sci. USA **112**, E1038 (2015).

[35] N. Giordano, F. Mairet, J.-L. Gouzé, J. Geiselmann, and H. De Jong, Dynamical allocation of cellular resources as an optimal control problem: Novel insights into microbial growth strategies, PLoS Comput. Biol. **12**, e1004802 (2016).

[36] D. W. Erickson, S. J. Schink, V. Patsalo, J. R. Williamson, U. Gerland, and T. Hwa, A global resource allocation strategy governs growth transition kinetics of escherichia coli, Nature (London) **551**, 119 (2017).

[37] M. Mori, S. Schink, D. W. Erickson, U. Gerland, and T. Hwa, Quantifying the benefit of a proteome reserve in fluctuating environments, Nat. Commun. **8**, 1225 (2017).

[38] Y. K. Kohanim, D. Levi, G. Jona, B. D. Towbin, A. Bren, and U. Alon, A bacterial growth law out of steady state, Cell Reports **23**, 2891 (2018).

[39] B. Alberts, R. Heald, A. Johnson, D. Morgan, M. Raff, K. Roberts, and P. Walter, *Molecular Biology of the Cell*, 5th ed. (W. W. Norton & Company, New York, 2022).

[40] R. Balakrishnan, M. Mori, I. Segota, Z. Zhang, R. Aebersold, C. Ludwig, and T. Hwa, Principles of gene regulation quantitatively connect dna to rna and proteins in bacteria, Science **378**, eabk2066 (2022).

[41] J. Lin and A. Amir, Homeostasis of protein and mRNA concentrations in growing cells, Nat. Commun. **9**, 4496 (2018).

[42] A. W. Pountain, P. Jiang, T. Yao, E. Homaee, Y. Guan, K. J. McDonald, M. Podkowik, B. Shopsin, V. J. Torres, and I. Golding, Transcription–replication interactions reveal bacterial genome regulation, Nature (London) **626**, 661 (2024).

[43] I. Golding and A. Amir, *Colloquium:* Gene expression in growing cells: A biophysical primer, Rev. Mod. Phys. **96**, 041001 (2024).

[44] N. M. Belliveau, G. Chure, C. L. Hueschen, H. G. Garcia, J. Kondev, D. S. Fisher, J. A. Theriot, and R. Phillips, Fundamental limits on the rate of bacterial growth and their influence on proteomic composition, Cell Syst. **12**, 924 (2021).

[45] A. Cylke, D. Serbanescu, and S. Banerjee, Energy allocation theory for bacterial growth control in and out of steady state, Proc. R. Soc. A: Math. Phys. Engn. Sci. **480**, 20240219 (2024).

[46] Y. Taniguchi, Quantifying e. coli proteome and transcriptome with single-molecule sensitivity in single cells, Seibutsu Butsuri **51**, 136 (2011).

[47] I. M. Keseler, Ecocyc: A comprehensive database resource for *Escherichia coli*, Nucleic Acids Res. **33**, D334 (2004).

[48] D. N. Wilson and K. H. Nierhaus, The ribosome through the looking glass, Angew. Chem. Int. Ed. **42**, 3464 (2003).

[49] A. Tiessen, P. Pérez-Rodríguez, and L. J. Delaye-Arredondo, Mathematical modeling and comparison of protein size distribution in different plant, animal, fungal and microbial species reveals a negative correlation between protein size and protein number, thus providing insight into the evolution of proteomes, BMC Res. Notes **5**, 85 (2012).

[50] J. Collier, Regulation of chromosomal replication in caulobacter crescentus, Plasmid **67**, 76 (2012).

[51] Y. Kitahara, E. R. Oldewurtel, S. Wilson, Y. Sun, S. Altabe, D. de Mendoza, E. C. Garner, and S. van Teeffelen, The role of cell-envelope synthesis for envelope growth and cytoplasmic density in *Bacillus subtilis*, PNAS Nexus **1**, pgac134 (2022).

[52] A. Schmidt, K. Kochanowski, S. Vedelaar, E. Ahrné, B. Volkmer, L. Callipo, K. Knoops, M. Bauer, R. Aebersold, and M. Heinemann, The quantitative and condition-dependent *Escherichia coli* proteome, Nat. Biotechnol. **34**, 104 (2016).

[53] X.-P. Hu, B. Brahmantio, K. Bartoszek, and M. J. Lercher, Most bacterial gene families are biased toward specific chromosomal positions, Science **388**, 186 (2025).

[54] Y.-J. Sun, F. Bai, A.-C. Luo, X.-Y. Zhuang, T.-S. Lin, Y.-C. Sung, Y.-L. Shih, and C.-J. Lo, Probing bacterial cell wall growth by tracing wall-anchored protein complexes, Nat. Commun. **12**, 2160 (2021).

[55] https://github.com/BanerjeeLab/Gene_expression_bacterial_growth.

[56] I. D. Burdett, T. B. Kirkwood, and J. B. Whalley, Growth kinetics of individual *Bacillus subtilis* cells and correlation with nucleoid extension, J. Bacteriol. **167**, 219 (1986).